11-28-2011

Modeling Free-carrier Absorption and Avalanching by Ultrashort Laser Pulses

Jeremy R. Gulley
Kennesaw State University, jgulley@kennesaw.edu

Modeling free-carrier absorption and avalanching by ultrashort laser pulses

Jeremy R. Gulley

Kennesaw State University, Department of Biology and Physics,
1000 Chastain Rd., Building 12, Room 308, Kennesaw, GA 30144, USA

ABSTRACT

In the past decade it was demonstrated experimentally that negatively-chirped laser pulses can lower the surface LIDT for wide band-gap materials by decreasing the number of photons required for photoionization on the leading edge of the pulse. Similarly, simulations have shown that positively-chirped pulses resulting from self-focusing and self-phase modulation in bulk dielectrics can alter the onset of laser-induced material modifications by increasing the number of photons required for photoionization on the leading edge of the pulse. However, the role of multi-chromatic effects in free-carrier absorption and avalanching has yet to be addressed. In this work a frequency-selective model of free-carrier dynamics is presented, based on a recently extended multi-rate equation for the distribution of electrons in the conduction band. In this model free-carriers gain energy from the field by single-photon absorption at the instantaneous frequency, which varies as a function of space and time. For cases of super-continuum generation it is shown that a Drude-type absorption can vary from 50% to over 200% the absorption rate as evaluated at the central pulse frequency only. Simulations applying this model to ultrafast laser-plasma interactions in fused silica explore how pulse chirps may be used as a distinguishing parameter for LID resulting from otherwise identical pulses.

Keywords: Ultrashort pulse propagation, simulation, free-carrier absorption, ionization, chirped laser pulse, nonlinear optics, SPIE Proceedings, fused silica

1. INTRODUCTION

High-intensity ultrashort laser pulses are now used to affect a variety of modifications to both dielectrics and semiconductors.[1–5] The short duration of these pulses typically allows the user to ignore coupling of thermal and optical effects, leading to clean, repeatable modifications and damage sites. Although thermal coupling and other potential complications are sometimes included when modeling ultrafast laser-induced damage, the issue of spectral effects receives comparatively little attention.[6] This is likely due to the fact that in a transform-limited pulse, with a temporal width on the order of 100 fs, the bandwidth is much smaller than the carrier frequency itself, and therefore the frequency dependent optical parameters are not expected to vary significantly over such a small range. For models of laser-energy absorption and damage, as long as a pulse's spectrogram remains symmetric about a central frequency, then violating the monochromatic assumption would not change the absorption process significantly, as the absorption of lower energy photons would tend to be offset by the absorption of an equal number of correspondingly higher energy photons.

Such is not the case, however, for strongly chirped pulses. Figure 1a shows the spectra for a 100 fs transform-limited pulse and a negatively-chirped pulse, both centered at a wavelength of 800 nm. Although both plots in Fig. 1a represent pulses of equal temporal width and energy, the negatively-chirped pulse spectrum is identical to that of a transform-limited 10 fs pulse. Unlike a 10 fs transform-limited pulse, however, the spectrogram of the negatively-chirped pulse is not symmetric about the 800 nm wavelength. Spectral variations of the kind seen in Fig. 1a are a simple matter to control if one is interested only in laser-induced modifications on a material surface. For modifications in the bulk, however, nonlinear optical effects can chirp the pulse and distort the spectrum significantly during propagation, even for initially transform-limited pulses (see Fig. 1b). Therefore, to model laser-induced damage by chirped pulses, a multi-chromatic approach must be taken. In this work, the instantaneous frequency is used as a measure of the average frequency at a given time. Existing models of

Further author information: Jeremy R. Gulley: E-mail: jgulley@kennesaw.edu, Telephone: 1 678 797 2933

Laser-Induced Damage in Optical Materials: 2011, edited by Gregory J. Exarhos,
Vitaly E. Gruzdev, Joseph A. Menapace, Detlev Ristau, M. J. Soileau, Proc. of SPIE Vol. 8190
819022 · © 2011 SPIE · CCC code: 0277-786X/11/$18 · doi: 10.1117/12.899257

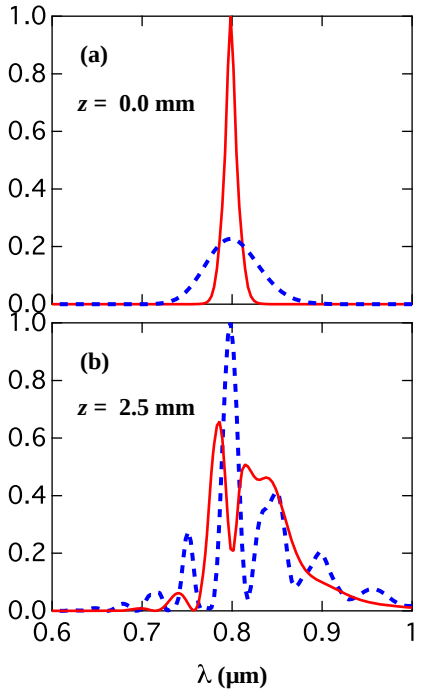

Figure 1. (a) Spectra for a 100 fs transform-limited pulse (solid red line) and a 100 fs negatively-chirped laser pulse (dashed blue line), both centered at 800 nm. (b) The on-axis spectra for the initially 100 fs transform-limited (solid red line) and negatively-chirped (dashed blue line) pulses after coming to a focus through 2.5 mm of fused silica.

photoionization and free-carrier dynamics in the conduction band are modified to allow the absorption of photon energies that vary as a function of time. In particular, an extended multi-rate equation[7] is used to model multi-chromatic free-carrier absorption in the conduction band. These models are used to simulate the propagation of unchirped, negatively-chirped and positively-chirped laser pulses to a focus through 2.5 mm of fused silica glass. The multi-chromatic effects of free-carrier absorption are shown to change the peak-ionization yields by a factor of two or greater.

2. THEORY

In this work multi-chromatic models of both photoionization and free-carrier absorption (a prerequisite process for avalanching) are introduced. The initial generator of free-carriers is taken to be photoionization, after which freed electrons may absorb single photons of energy $\hbar\omega_\tau$ where ω_τ is the instantaneous frequency. Additionally, the rate of 1-photon absorption by conduction-band electrons will be derived directly from the propagation equation, thus ensuring agreement between the models of plasma and field evolution. These models (including the treatment of multi-chromatic effects) constitute a time-domain description of the behavior. They are not a true frequency description of the behavior, which would require working in the Fourier space. The modified models are intended to provide a quantitative estimate of the importance of multi-chromatic effects in bulk propagation, since a frequency-domain treatment of plasma generation is not available at this time.

2.1 Photoionization

For the simulations presented in this paper, the Keldysh photoionization rate for solids[8] is used because in numerous studies it has provided good agreement with experiments of ultrashort laser pulse propagation in fused silica,[9–18] and fused silica will be the material referenced in this work. The Keldysh photoionization formula for

a field of complex amplitude ξ with frequency ω in a solid of band gap U and reduced electron-hole mass m_r is:[8]

$$W_{\text{PI}}(|\xi|,\omega;U,m_r)=\frac{2\omega}{9\pi}\left(\frac{m_r\omega}{\sqrt{\gamma_1}\,\hbar}\right)^{3/2}Q(\gamma,x)\exp\left(-\varpi\left\langle x+1\right\rangle\right). \tag{1}$$

Here the Keldysh parameter $\gamma=\omega\sqrt{m_rU/e}\,|\xi|$, $\gamma_1=\gamma^2/(1+\gamma^2)$, $\varpi=\pi\left(K(\gamma_1)-E(\gamma_2)\right)/E(\gamma_2)$, $\gamma_2=1-\gamma_1$, and $x=(2U/\pi\omega)(\sqrt{1-\gamma^2}/\gamma)E(\gamma_2)$. The functions $K(x)$ and $E(x)$ are complete elliptical integrals of the first and second kind, respectively, as defined in Ref. 19. The function $Q(\gamma,x)$ is given by

$$Q(\gamma,x)=\sqrt{\frac{\pi}{2K(\gamma_2)}}\sum_{n=0}^{\infty}\exp\left(-n\varpi\right)\Phi\left(\sqrt{\vartheta(n+2\nu)}\right),$$

where $\vartheta=\pi^2/4K(\gamma_2)E(\gamma_2)$, $\nu=\left\langle x+1\right\rangle-x$, $\langle\cdot\rangle$ denotes the integer part, and $\Phi(z)=\int_0^z\exp(y^2-z^2)dy$ is the Dawson function. The multi-chromatic photoionization rate is calculated by using the instantaneous frequency $\omega_\tau=\omega_0-\Im[(\partial_\tau\xi)/\xi]$ in Eq. (1), where the notation $\Im[\cdot]$ denotes the imaginary part. For the case of a negatively-chirped laser pulse, the blue-shifted photons on the leading pulse edge lead to higher photoionization rates earlier in the laser pulse, giving more time for impact ionization to raise the total ionization yield. The opposite situation occurs for a positively-chirped laser pulse, where red-shifted photons on the leading pulse edge lowers the photoionization rate there, giving less time for impact ionization. The importance of this effect was verified experimentally when it was shown that the surface damage threshold for fused silica was up to 20% lower for a negatively-chirped ultrashort laser pulse, as compared to that of an otherwise identical positively-chirped pulse.[20]

2.2 Free-carrier absorption and avalanching

There are numerous models available to describe free-carrier dynamics in the conduction band. These range from complex models describing the time evolution of the electron distribution such as the Boltzmann equation,[15] the Fokker-Planck equation,[21–23] and Monte-Carlo methods,[24] to comparatively simpler methods such as Stuart's single rate equation for the free-electron density.[23] In the past decade, a multi-rate equation (MRE) model[25,26] was developed to merge the simplicity of the single-rate equation approach with the completeness of a free-electron distribution model. In the MRE model, discrete electron populations in the conduction band are separated in energy by amounts of $\hbar\omega$, where ω is the frequency of the applied field. More recently, the MRE was extended by making the energy spacing between electron populations equal to the mean phonon energy.[7] This allowed for inclusion of the energy loss from free-carriers to the phonon gas, as well as Auger decay.

The extended MRE was originally developed as a description of free-electron behavior in semiconductors. However, in this work it is used because it allows conduction-band electrons to absorb photon energies that vary as a function of time. If the Auger process is neglected, the extended MRE is:[7]

$$\begin{aligned}\dot{n}_i &= W_{\text{PI}}\delta_{p,i}+\left[W_{i-k}^{pt}n_{i-k}\theta(\epsilon-\hbar\omega_\tau)-W_i^{pt}n_i\right] \\ &\quad+\left[\frac{n_{i+1}}{\tau_{i+1}^{pn}}(1-\delta_{i,m})-\frac{n_i}{\tau_i^{pn}}\right]+\left[\sum_{l=j}^{m}\alpha_l n_l\delta_{i,1}+\alpha_{i+j}n_{i+j}-\alpha_i n_i\theta(\epsilon_i-\epsilon_c)\right]\end{aligned} \tag{2}$$

where all the variables, indices, and accompanying parameters are defined in Table 1. The formulas to calculate $\tilde{\Delta}$, ϵ_{PI}, ϵ_c are all taken from Ref. 15. The terms on the right-hand side of Eq. (2) are, from left to right, a photoionization contribution into the ϵ_p energy level, a free-carrier absorption contribution taking electrons away from the ϵ_i level and promoting electrons from the ϵ_{i-k} level, an electron-phonon collision term accounting for electron energy loss into the phonon gas, and the avalanching contribution whereby electrons with energy exceeding ϵ_c may impact a valance electron and promote it to the conduction band, losing an energy equal to the band gap U in the process. The energy dependence of the impact ionization rate α_i is given by the Keldysh impact ionization formula $\alpha_i=P\left((\epsilon_i-\epsilon_c)/\epsilon_c\right)^2\Theta(\epsilon_i-\epsilon_c)$, where $\Theta(x)$ is the Heaviside step function. This work assumes that the rate coefficient $P=1.5$ fs^{-1}, which is also taken from Ref. 15.

Table 1. Summary of the variables, indices, and parameters for the extended multi-rate equation

Symbol	*Description*
n_i	Free-electron density with energy ϵ_i
ϵ_i	Free-electron energy
i	Energy index
m	Maximum energy index
j	$\langle \epsilon_c/\Delta\epsilon \rangle + 1$
k	$\langle \hbar\omega_\tau/\Delta\epsilon \rangle + 1$
p	$\langle \epsilon_{\rm PI}/\Delta\epsilon \rangle + 1$
U	Material band gap
$\tilde{\Delta}$	Effective band gap
$\epsilon_{\rm PI}$	Energy remaining after photoionization
ϵ_c	Critical energy for impact ionization
$W_{\rm PI}$	Photoionization rate
W_i^{pt}	1-photon absorption rate
τ_i^{pn}	Electron-phonon collision rate
α_i	Impact ionization rate
$\Delta\epsilon$	Energy spacing (Mean phonon energy)

2.3 Ultrashort pulse propagation.

The modeling of pulse propagation is performed by solving for the complex envelope ξ of the linearly-polarized, cylindrically-symmetric electric field $\vec{E}$, defined by

$$\vec{E}(r,z,t) = \frac{1}{2}\left(\xi(r,z,t)\, e^{i(k_0 z - \omega_0 t)} + \text{c.c.}\right)\hat{x}\ .$$

The equation of propagation is derived in Ref. 27 and describes the evolution of ξ along the propagation axis z in the retarded time frame of the laser pulse, that is $\tau = t - z/v_g$, moving at the group velocity v_g.

$$\begin{aligned}\frac{\partial \xi}{\partial z} &= \frac{i}{2k_0}\hat{T}^{-1}\nabla_\perp^2\xi + i\hat{D}_b\xi + i\frac{k_0\epsilon_0 c n_2}{2}\hat{T}\left[\int_{-\infty}^{\tau} d\tau' R(\tau-\tau')\left|\xi(\tau')\right|^2\right]\xi \\ &\quad -\frac{W_{\rm PI}U}{2\,I}\,\xi - \sum_i\left[\frac{\sigma_i}{2}\,(1+i\omega_0\tau_{\rm c}(\epsilon_i))\,\hat{G}_i^{-1}\left[n_i\xi\right]\right]\end{aligned} \tag{3}$$

Here $\hat{D}_b$ is a bound-charge linear dispersion operator, $\hat{T}$ is a steepening operator, and $\hat{G}_i$ is a free-carrier dispersion operator, respectively defined as

$$\hat{D}_b = \sum_{m=2}^{\infty}\frac{k_m}{m!}(i\partial_\tau)^m,\quad \hat{T} = 1 + i\tfrac{1}{\omega_0}\partial_\tau,\quad \text{and}\quad \hat{G}_i = 1 + i\frac{g_i}{\omega_0}\partial_\tau,$$

where linear absorption due to bound charges is neglected.

The first term on the right hand side of Eq. (3) accounts for diffraction and linear shock, the second term accounts for dispersion due to bound charges, the third term represents contributions from the nonlinear polarization, the fourth term accounts for absorption due to photoionization, and the fifth term includes free-carrier absorption and plasma defocusing. The delayed nonlinear optical response function $R(\tau)$ is given by,[29]

$$R(\tau) = (1-f_r)\delta(\tau) + f_r\frac{\tau_1^2+\tau_2^2}{\tau_1\tau_2^2}\,e^{-\tau/\tau_2}\,\sin(\tau/\tau_1),$$

where the first term is an instantaneous electronic response, f_r is the fraction of the Raman contribution to the nonlinear polarization, and the constants τ_1 and τ_2 are adjustable parameters chosen to provide an adequate fit

Table 2. Summary of the variables and parameters for the propagation equation.

Symbol	*Description*	*Definition*
ξ	Electric field envelope	
r	Beam radius coodrinate	
z	Propagation axis coordinate	
τ	Retarded time coordinate	
ω_0	Carrier frequency	
k	Wave vector	
k_m	m^{th} order dispersion coefficient	$\partial k/\partial\omega)_{\omega_0}$
σ_i	Free-carrier absorption cross section	$e^2\tau_\mathrm{c}(\epsilon_i)/n_0 c\epsilon_0 m_e(1+\omega_0^2\tau_\mathrm{c}^2(\epsilon_i))$
g_i	Free-carrier dispersion constant	$(-i\omega_0\tau_\mathrm{c}(\epsilon_i))\,/\,(1-i\omega_0\tau_\mathrm{c}(\epsilon_i))$
I	Field intensity	$I=(1/2)n_0\epsilon_0 c\lvert\xi\rvert^2$

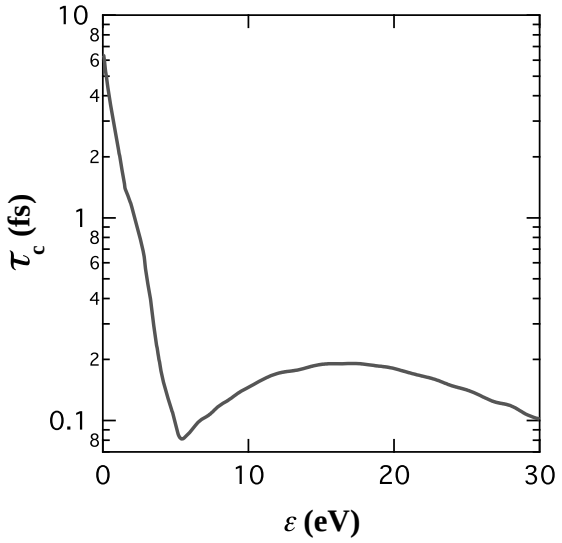

Figure 2. Collision time given as a function of electron energy in the conduction band.[28]

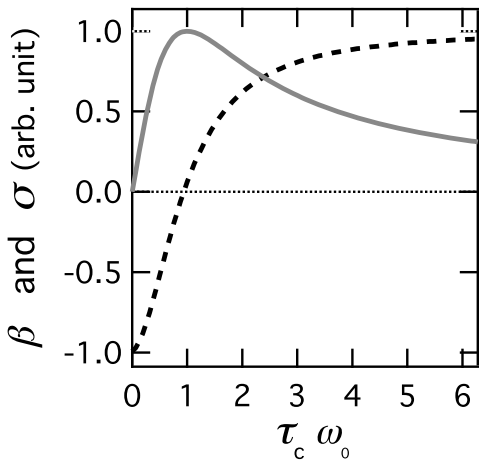

Figure 3. The parameter β and the normalized Drude free-carrier collision cross-section σ, as a function of collision time τ_c, in proportion to the chosen carrier frequency ω_0. Both β and σ are energy dependent via their dependence on $\tau_c(\epsilon_i)$.

with the Raman-gain spectrum. The nonlinear polarization term in Eq. (3) collectively accounts for self-focusing, self-phase modulation, self-steepening, and stimulated Raman scattering.

The last term in Eq. (3) is calculated by using a Drude model for the free-current density contribution of free-carriers at each electron energy ϵ_i,

$$\frac{\partial \vec{J}_i}{\partial t} = -\frac{\vec{J}_i}{\tau_c(\epsilon_i)} + \frac{e^2}{m_e(\epsilon_i)} n_i \vec{E}, \tag{4}$$

where the index i is the same energy-level index as defined in Table 1 for Eq. (2). For the remainder of this work, the effective electron mass is taken to be the rest electron mass, while the momentum relaxation time as a function of electron energy is taken from Ref. 28 and is plotted in Fig. 2. Note that Eq. (4) describes the time-evolution of the free-current density for the ϵ_i electron energy population only, and must be summed over all energy levels to yield the total free-current density. Hence, this summation occurs explicitly in the last term of Eq. (3).

The operator $\hat{G}^{-1}$ in Eq. (3) is a direct result of solving Eq. (4) for a non-monochromatic pulse where the total free-carrier density can vary significantly over comparatively short periods of time. If $\hat{G}^{-1}$ is expanded and truncated at first order, one can determine that the time-averaged energy per time per volume lost from the field into the free-carrier population at energy ϵ_i is[27]

$$\left[\frac{\partial I}{\partial z}\right]_i^{(\mathrm{fc})} = -\sigma_i n_i I - \sigma_i \tau_{c_i} \beta_i I \left[\dot{n}_i\right] - \sigma_i \tau_{c_i} \beta n_i \left[\frac{\dot{I}}{2}\right] - \sigma_i (\beta_i + 1) n_i I \left[\frac{\omega_0 - \omega_\tau}{\omega_0}\right]. \tag{5}$$

Here, the energy dependent constant $\beta_i = (\omega_0^2 \tau_c^2(\epsilon_i) - 1)/(\omega_0^2 \tau_c^2(\epsilon_i) + 1)$ is plotted, along with the Drude cross-section of absorption, in Fig. 3. The first term in Eq. (5) is the ordinary Drude absorption. The remaining terms (from left to right) are ultrashort corrections to absorption resulting from a time-variable free-carrier density, broad spectral widths, and strong pulse chirps. Note in Fig. 3 that the constant β_i can be less than zero for small values of the momentum relaxation time. For visible and near-IR fields, this change of sign will occur for $\tau_c \ll 1$ fs, which is the case for much of the conduction band as demonstrated by Fig. 2, effectively reversing the contribution of those corrective terms so that they reduce the amount of energy absorbed by the field.

The transfer of pulse energy in Eq. (5) to electrons at energy ϵ_i by photons of energy $\hbar\omega_\tau$ must equal $\hbar\omega_\tau \left[\dot{n}_i\right]^{(\mathrm{fc})}$. Therefore, an effective 1-photon absorption coefficient can be calculated from Eq. (5) for use in Eq. (2) that is consistent with the ultrashort temporal corrections intrinsic to Eq. (3). Using this method, one can ensure that the pulse propagation equation and the plasma evolution model agree on the amount of energy deposited into the material, which is not currently the case for most calculations in the literature.

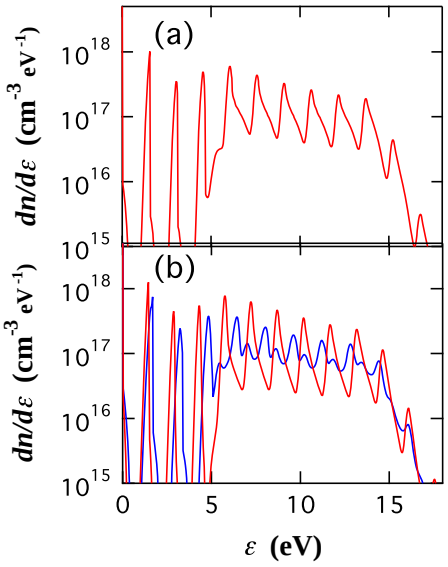

Figure 4. Distributions of free-carriers in the conduction band at the trailing edge of an (a) unchirped pulse, (b) a positively-chirped pulse, red line, and negatively-chirped pulse, blue line. All pulses were 100 fs in duration with the same total energy.

3. MULTI-CHROMATIC EFFECTS ON THE ELECTRON DISTRIBUTION

To see multi-chromatic effects on the electron distribution in the conduction band, it is instructive to examine the distribution after exposure to unchirped vs chirped pulses. Figure 4 shows solutions of Eq. (2) on the trailing edge ($\tau = +100$ fs) of a 100 fs Gaussian laser pulse, with a peak intensity of 6×10^{12} W cm^{-2}, for different chirps. The chirp parameters of each pulse are zero for the unchirped pulse, $+10^{27}$ s^{-1} for the positively-chirped pulse, and -10^{27} s^{-1} for the negatively-chirped pulse, giving the respective spectra seen in Fig. 1a. The exposed material is fused silica, with an assumed band gap of 9 eV and mean phonon energy of 0.033 eV. The energy dependent free-carrier absorption rate for Eq. (2) was calculated from Eq. (5), where electrons absorbed photons of the instantaneous frequency ω_τ.

The total plasma densities for the respective plots in Fig. 4 are all approximately 5.1×10^{18} cm^{-3}, differing from each other by only a few percent. The contribution of photoionization is approximately the same regardless of pulse chirp for the cases presented because the chirp is smallest at the temporal center where the intensity is largest. However, the shapes of the distributions on the trailing edge are significantly different, particularly between distributions resulting from the positively and negatively-chirped pulses. This is due to the fact that the positively-chirped laser pulse solution (blue line) has a higher spacing in between the absorption peaks due to the blue shifting (and therefore higher photon energies) on the trailing edge, as opposed to the red shifting (lower photon energies) on the trailing edge of the negatively-chirped pulse. Due to the energy dependence of collision times and effective masses, changes in optical properties of the free electron gas are allowed to develop as a result.

4. ULTRASHORT PULSE PROPAGATION IN FUSED SILICA

The simulations begin by constructing the electric field envelope at the beginning of the propagation according to the formula

$$\xi(r, \tau, z = -f) = \sqrt{\frac{2I_0}{\epsilon_0 c}} \exp\left(-\frac{r^2}{w_r^2} - i\frac{k_0 r^2}{2f} - \frac{\tau^2}{\tau_0^2}\right),$$

where $I_0 = E_0/(\pi/2)^{3/2}\omega_r^2\tau_0$ is the initial peak intensity, and all other parameters are defined in Table 3. The geometric focus of the laser beam is placed 3 mm into the bulk of a fused silica sample to preclude any

Table 3. Numerical values used in all the simulations reported in this work. Material parameters are those for fused silica.

Symbol	*Description*	*Value*	*Units*
λ	Initial wavelength	800	nm
τ_0	Initial pulsewidth	100	fs
w_r	Initial beam waist	2	mm
E_0	Initial pulse energy	750	nJ
f	Lens focal length	25	cm
L_z	Sample length	2.5	mm
n_0	Linear refractive index	1.45	
n_2	Nonlinear refractive index	2.48×10^{-16}	cm^2W^{-1}
f_r	Raman response fraction	0.18	
τ_1	Raman sinusoidal time	12.2	fs
τ_2	Raman decay time	32	fs
U	Material band gap	9	eV
m_e	Effective electron mass	9.11×10^{-31}	kg
m_r	Reduced electron-hole mass	4.56×10^{-31}	kg
$\Delta\epsilon$	Mean phonon energy	0.033	eV

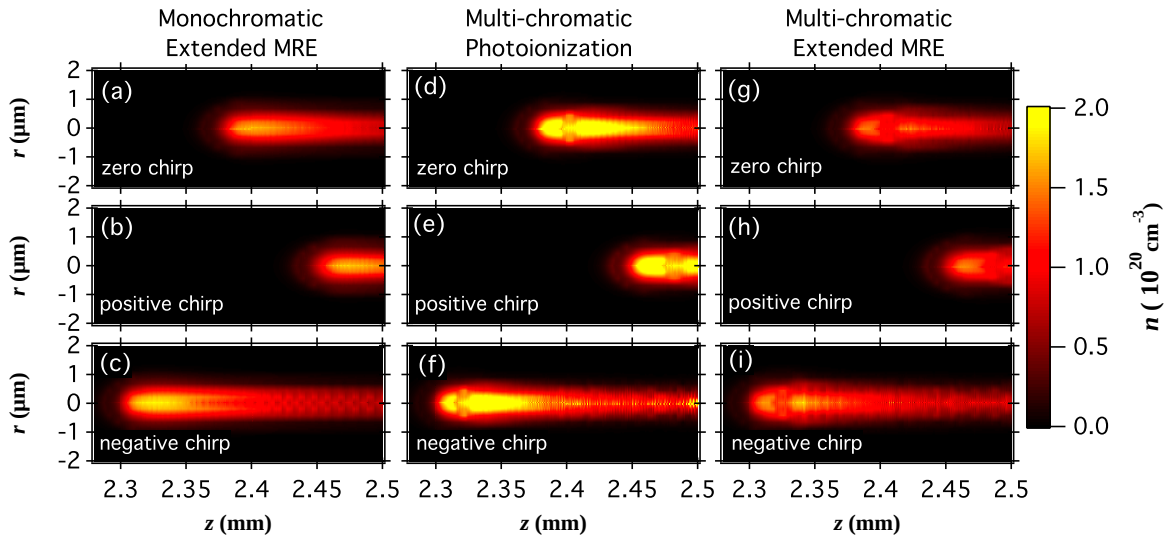

Figure 5. Peak plasma density plots obtained by solving Equations (2) and (3). (a)-(c) respectively show the unchirped, positively-chirped and negatively-chirped pulse solutions for a complete monochromatic treatment of Equation (2). (d)-(f) respectively show the unchirped, positively-chirped and negatively-chirped pulse solutions for a monochromatic treatment of Equation (2), except for the photoionization rate. (g)-(i) respectively show the unchirped, positively-chirped and negatively-chirped pulse solutions for a complete multi-chromatic treatment of Equation (2).

surface damage effects. The pulse is numerically focused and the resulting peak plasma generation in the bulk is recorded as a function of beam position and propagation distance in Fig. 5. The peak plasma densities recorded in Fig. 5 are below those typically associated with permanent damage, but have been correlated with reversible modifications to the medium.

Note that all the pulses focus in the material and generate optically appreciable plasma densities before the geometric focus at 3mm into the material is reached. This is due to catastrophic self-focusing driven by the nonlinear Kerr effect. Note also that the negatively-chirped pulses come to a focus earlier in the material. This is due to the effect of linear dispersion causing the negatively-chirped pulse to compress in addition to self-focusing, while dispersion works to somewhat broaden the positively-chirped pulse, slightly delaying the

self-focusing process. In each case the location of the potential bulk modification is determined to a high degree of precision by the multi-chromatic linear dispersion effects only, and not by the multi-chromatic plasma effects.

Once the propagation effects bring the pulse to a focus, however, the density of free-carriers generated, as well as the structure of the potential bulk modification, are significantly influenced by the multi-chromatic plasma effects. As can be seen by comparison of the plots (a)-(c) with the plots (d)-(f) which include multi-chromatic effects in photoionization only, the shape of the peak plasma distribution is altered and the corresponding peak densities increase noticeably. Further comparison of the plots (d)-(f) with the plots (g)-(i), which use the full multi-chromatic version of Eq. (2), shows that a multi-chromatic approach to free-carrier absorption significantly reduces the overall 1-photon absorption rate and resulting avalanche yields. The net effect of this reduction is to reduce much of the maximum plasma densities by a factor of two or greater. This effect results from the temporal corrections found in Eq. (5), as well as the altered optical properties made possible by the chromatic-induced change in energy distribution of free-carriers as shown in Fig. 4. These effects are especially important for the plasma generation occurring near the beam center, or any forming filament, where the intensities are highest and the spectral composition is the most distorted (see Fig. 1b).

5. CONCLUSION

Simulations of multi-chromatic laser-induced ionization have been performed for fused silica glass. These are the first calculations of their kind in that they attempt to model both the fully three-dimensional pulse propagation and plasma generation of single-shot non-monochromatic radiation, and of chirped pulses in particular. This is exceptionally important for bulk propagation, where strong pulse chirps are inevitable due to nonlinear optical effects. For this purpose, the extended multi-rate equation is modified to allow free-carrier absorption of photons with time-variable energies and absorption rates. This alters the general shape of the free-carrier distribution in the conduction band and (combined with the multi-chromatic effects of propagation and photoionization), leads to measurable changes in the location, shape, and severity of material modifications which would be impossible to predict without this treatment. The lowering (and in some places raising) of ionization yields by a factor of 2 or greater, as well as the precise influence over location of bulk modifications, suggests that pulse chirps could be used as a possible parameter for laser-induced damage from otherwise identical pulses.

The changes resulting from the inclusion of multi-chromatic plasma effects in the presented data are a quantitative estimate, since the inclusion of multiple frequencies was modeled with a time-domain approach using the instantaneous frequency. A true quantitative model of multi-chromatic effects must involve either a non-time averaged treatment in the time-domain or a full frequency treatment in the Fourier-domain. Such a description will be necessary in the future to accurately model the generation of free-electrons from chirped pulses in dielectrics, or ionization by any high intensity laser pulse that is influenced by nonlinear optical effects in the bulk.

ACKNOWLEDGMENTS

The author would like to thank CETL at Kennesaw State University for the funding of this work.

REFERENCES

[1] Vogel, A., Noack, J., Huttman, G., and Paltauf, G., "Mechanisms of femtosecond laser nanosurgery of cells and tissues," *Appl. Phys. B* **81**, 1015–1047 (Dec 2005).

[2] Schaffer, C. B., Brodeur, A., Garcia, J. F., and Mazur, E., "Micromachining bulk glass by use of femtosecond laser pulses with nanojoule energy," *Opt. Lett.* **26**, 93–95 (Jan 2001).

[3] Cerami, L. R., Mazur, E., Nolte, S., and Schaffer, C. B., "Femtosecond laser micromachining," in [*Ultrafast Optics*], Trebino, R. and Squier, J., eds., 1–1, Trafford Publishing (2007).

[4] Gattass, R. R., Cerami, L. R., and Mazur, E., "Micromachining of bulk glass with bursts of femtosecond laser pulses at variable repetition rates," *Opt. Exp.* **14**, 5279–5284 (2006).

[5] Zhu, X., Naumov, A. Y., Villeneuve, D. M., and Corkum, P. B., "Influence of laser parameters and material properties on micro drilling with femtosecond laser pulses," *Appl. Phys. A* **V69**(0), S367–S371 (1999).

[6] Gulley, J. R., "Frequency dependence in the initiation of ultrafast laser-induced damage," in [*Laser-Induced Damage in Optical Materials: 2010*], Exarhos, G. J., Gruzdev, V. E., Menapace, J. A., Ristau, D., and Soileau, M. J., eds., *Laser-Induced Damage in Optical Materials: 2010* **7842**(1), 78420U, SPIE (2010).
[7] Medvedev, N. and Rethfeld, B., "A comprehensive model for the ultrashort visible light irradiation of semiconductors," *J. Appl. Phys.* **108**(10), 103112 (2010).
[8] Keldysh, L. V., "Ionization in the field of a strong electromagnetic wave," *Sov. Phys. JETP* **20**(5), 1307 (1965).
[9] Berge, L., Skupin, S., and Steinmeyer, G., "Temporal self-restoration of compressed optical filaments," *Phys. Rev. Lett.* **101**(21), 213901 (2008).
[10] Couairon, A., Sudrie, L., Franco, M., Prade, B., and Mysyrowicz, A., "Filamentation and damage in fused silica induced by tightly focused femtosecond laser pulses," *Phys. Rev. B* **71**(12), 125435 (2005).
[11] Sudrie, L., Couairon, A., Franco, M., Lamouroux, B., Prade, B., Tzortzakis, S., and Mysyrowicz, A., "Femtosecond laser-induced damage and filamentary propagation in fused silica," *Phys. Rev. Lett.* **89**, 186601 (Oct 2002).
[12] Winkler, S. W., Burakov, I. M., Stoian, R., Bulgakova, N. M., Husakou, A., Mermillod-Blondin, A., Rosenfeld, A., Ashkenasi, D., and Hertel, I. V., "Transient response of dielectric materials exposed to ultrafast laser radiation," *Appl. Phys. A* **V84**(4), 413–422 (2006).
[13] Wu, A. Q., Chowdhury, I. H., and Xu, X., "Femtosecond laser absorption in fused silica: Numerical and experimental investigation," *Phys. Rev. B* **72**(8), 085128 (2005).
[14] Christensen, B. H. and Balling, P., "Modeling ultrashort-pulse laser ablation of dielectric materials," *Phys. Rev. B* **79**(15), 155424 (2009).
[15] Kaiser, A., Rethfeld, B., Vicanek, M., and Simon, G., "Microscopic processes in dielectrics under irradiation by subpicosecond laser pulses," *Phys. Rev. B* **61**, 11437–11450 (May 2000).
[16] Liu, J., Li, R., and Xu, Z., "Few-cycle spatiotemporal soliton wave excited by filamentation of a femtosecond laser pulse in materials with anomalous dispersion," *Phys. Rev. A* **74**(4), 043801 (2006).
[17] Mero, M., Liu, J., Rudolph, W., Ristau, D., and Starke, K., "Scaling laws of femtosecond laser pulse induced breakdown in oxide films," *Phys. Rev. B* **71**(11), 115109 (2005).
[18] Polesana, P., Dubietis, A., Porras, M. A., Kucinskas, E., Faccio, D., Couairon, A., and Trapani, P. D., "Near-field dynamics of ultrashort pulsed bessel beams in media with kerr nonlinearity," *Phys. Rev. E* **73**(5), 056612 (2006).
[19] Abramowitz, M. and Stegun, I. A., [*Handbook of Mathematical Functions*], Dover, New York, tenth ed. (1964).
[20] Louzon, E., Henis, Z., Pecker, S., Ehrlich, Y., Fisher, D., Fraenkel, M., and Zigler, A., "Reduction of damage threshold in dielectric materials induced by negatively chirped laser pulses," *Appl. Phys. Lett.* **87**(24), 241903 (2005).
[21] Holway, L. H., "High-frequency breakdown in ionic crystals," *J. Appl. Phys.* **45**(2), 677–683 (1974).
[22] Sparks, M., Mills, D. L., Warren, R., Holstein, T., Maradudin, A. A., Sham, L. J., Loh, E., and King, D. F., "Theory of electron-avalanche breakdown in solids," *Phys. Rev. B* **24**, 3519–3536 (Sep 1981).
[23] Stuart, B. C., Feit, M. D., Herman, S., Rubenchik, A. M., Shore, B. W., and Perry, M. D., "Nanosecond-to-femtosecond laser-induced breakdown in dielectrics," *Phys. Rev. B* **53**, 1749–1761 (Jan 1996).
[24] Jacoboni, C. and Lugli, P., [*The Monte Carlo Method for Semiconductor Device Simulation*], Springer-Verlag/Wien (1998).
[25] Rethfeld, B., "Free-electron generation in laser-irradiated dielectrics," *Phys. Rev. B* **73**(3), 035101 (2006).
[26] Rethfeld, B., "Unified model for the free-electron avalanche in laser-irradiated dielectrics," *Phys. Rev. Lett.* **92**(18), 187401 (2004).
[27] Gulley, J. R. and Dennis, W. M., "Ultrashort-pulse propagation through free-carrier plasmas," *Phys. Rev. A* **81**, 033818 (Mar 2010).
[28] Arnold, D., Cartier, E., and DiMaria, D. J., "Acoustic-phonon runaway and impact ionization by hot electrons in silicon dioxide," *Phys. Rev. B* **45**(3), 1477–1480 (1992).
[29] Blow, K. J. and Wood, D., "Theoretical description of transient stimulated raman scattering in optical fibers," *J. Quant. Electr.* **25**, 2665–2673 (Dec. 1989).

8190 22
Modeling free-carrier absorption and avalanching by ultrashort laser pulses
[8190-48]

Questions and Answers

Q. Thank you for this interesting approach. I saw that you include the electron-phonon interaction in the model for propagation. Do the results depend on that? I believe that I have seen energy dependent electron-phonon interaction times.

A. You are correct. The ability to put that in the model is definitely there and my experience was that it did not change the results dramatically. I had tried it with a very basic model of the variation of that particular collision time and it did not affect the results tremendously, but the paper from which I got this information also has the same information for that collision time and it can be there in principle, but I've done other simulations similar to that and I did not see as big an effect. In fact, the big effect that is probably being ignored here relate to the electron-electron collisions which will spread the peaks out. And, I'm not yet aware of a good way to put that in.

Q. You said that you have used the free electron mass, I guess?

A. Yes.

Q. I was wondering if you tried to vary this a little bit and look at how this affects your results, like kind of a sensitivity test.

A. It's on the to do list, and I have not done it yet.